

Cavity-mediated coupling of antiferromagnetic spin waves

M. Białek,^{*,†,‡} W. Knap,[‡] and J.-Ph. Ansermet[†]

[†]*Institute of Physics, École Polytechnique Fédérale de Lausanne (EPFL), 1015 Lausanne,
Switzerland*

[‡]*Centera Laboratories, Institute of High Pressure Physics, Polish Academy of Sciences,
Warsaw 01-142, Poland*

E-mail: marcin.bialek@fuw.edu.pl

Abstract

Coupling of space-separated oscillators is interesting for quantum and communication technologies. In this work, it is shown that two antiferromagnetic oscillators placed inside an electromagnetic cavity couple cooperatively to its terahertz modes and, in effect, hybridized magnon-polariton modes are formed. This is supported by a systematic study of reflection spectra from two parallel-plane slabs of hematite (α -Fe₂O₃), measured as a function of their temperatures and separation distance, and modeled theoretically. The mediating cavity was formed by the crystals themselves and the experiment was performed in a practical distance range of a few millimetres and above room temperature. Cavity-mediated coupling allows for engineering of complex resonators controlled by their geometry and by sharing properties of their components.

1 Introduction

Strong coupling between light and matter states gives rise to hybridization into polariton states and Rabi oscillations.¹ Cooperative interaction of light with N resonators increases the splitting by a factor of \sqrt{N} , as was observed in a wide range of systems.²⁻⁶ With magnetic materials, strong coupling of microwave cavity modes and ferromagnetic resonance was observed as early as 1962,⁷ but this effect only gained broader attention in the 2010s,⁸⁻²⁰ because of the prospect of using magnetic polaritons in quantum devices.^{1,21-26} Coupling of matter states mediated by an electromagnetic cavity mode was shown in the case of mechanical oscillators.²⁷ Coupling of two ferromagnets mediated by a cavity mode was recently achieved experimentally using superconducting circuits^{28,29} and nanostripline antennas³⁰ and was also discussed theoretically.^{28,31-33} Furthermore, different magnon modes can also couple in some ferrimagnetic materials.³⁴ Most of these experiments require cryogenic temperatures and microwave radiation. Here, we demonstrate, above room temperature and in the terahertz (THz) range, cavity-mediated coupling of antiferromagnetic magnons in crystals separated by a well-controlled gap. Mediating cavity is a Fabry-Perot type cavity defined in part by these two crystals themselves. We used hematite (α -Fe₂O₃) that is characterised by very low spin damping.³⁵⁻³⁷ Its antiferromagnetic resonance (AFMR) frequency rises with temperature (above room temperature).³⁸ We show that our experimental data can be interpreted with a model based on the input-output theory, classical electrodynamics or a microscopic model. We find that, in the case of our setup, the maximal separation between samples with observable magnon-magnon coupling is in the easily-achievable millimeter range, that is up to ten times the thickness of slabs used in the experiment.

Antiferromagnets are of special interest³⁹⁻⁴¹ for spintronics and magnon-polariton research because frequencies of magnons in antiferromagnets reach the THz range and some phenomena occur in them that are unavailable in ferromagnets.⁴²⁻⁴⁴ Antiferromagnetic polaritons were achieved mostly at low frequencies,⁴⁵ in bulk samples^{46,47} or via an indirect coupling,^{48,49} whereas direct strong cavity-magnon coupling at high frequencies was shown

only very recently.⁵⁰ One of the reasons is the technical difficulty of constructing THz cavities of high-enough quality factor,⁵¹ as they need to be much smaller than the ones used in the microwave range. Here, we show that reflection from a Fabry-Perot type cavity shows strong coupling of its modes with AFMR. We show versatility of this scheme of observing magnetic polaritons by achieving coupling of AFMR in two spaced parallel-plane slabs of hematite.

2 Experimental

The experiment relies on a continuous-wave THz spectrometer based on frequency extenders linked to a vector network analyzers (VNA), characterized by a very high frequency resolution. Thanks to its very high dynamic range, we can detect AFMR even in transmission through absorptive samples.^{52–55} In this communication, we used an extender emitting linearly polarized and monochromatic radiation spanning from 0.2 to 0.35 THz. The extender probes S_{11} signal coming back to the emission antenna, thus allowing us to measure reflection at 0 deg incidence angle without any beam splitters.

We used two single crystals of natural hematite in [10-10] cut of 0.39, 0.5 mm in thickness and lateral dimensions of 10×10 mm². From the extender, the THz beam propagated toward the cavity using an oversized metallic waveguide. At its end, a hematite crystal of $h_W = 0.5$ mm thickness was placed (Fig. 1). This waveguide was mounted between Peltier elements that allowed temperature control of the sample mounted on its end. The second crystal of thickness $h_M = 0.39$ mm was placed on a copper mirror and its temperature was controlled with another Peltier element. Temperatures of both crystals were independently controlled and the size d of the air gap between the crystals was controlled with a motorized stage. Thermal transfer due to convection was small for $d > 0.2$ mm. In order to reduce possible temperature inhomogeneity of the crystal placed on the end of the waveguide, we chose temperatures as little as possible above room temperature, and the hematite AFMR fell in the spectral range of our extender (i.e. above 0.2 THz).

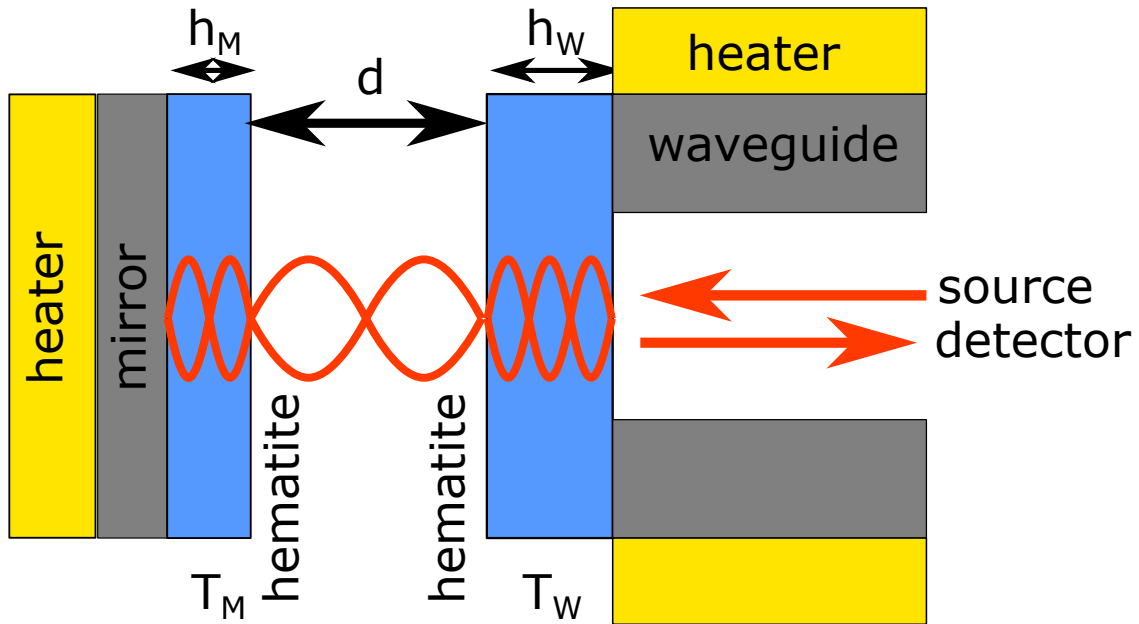


Figure 1: The measurement system comprises a hematite crystal of thickness h_M placed on a copper mirror and a second hematite crystal of thickness h_W placed at the end of an oversized copper waveguide. We measured reflection in the frequency range of 0.2 to 0.28 THz as a function of gap d between the crystals, imposing a temperature difference $\Delta T = T_M - T_W$, while keeping $T_M + T_W$ constant.

The detector measured the amplitude and phase of the reflected electric field E at the same polarization angle as that of the emitted beam. Spectra were collected as a function of gap d between the crystals for a fixed temperature difference $\Delta T = T_M - T_W$. Then, both temperatures were changed with a step of 0.25 K, keeping $T_M + T_W$ constant. This step was chosen so that the frequency change was smaller than the line width in the interaction region. Spectra were transformed in the time domain to cut-off reflection coming from the antenna itself and then transformed back into the frequency domain. Finally, magnitude data were divided by a reference spectrum, calculated as a median reflection for all values of d and ΔT . The power magnitude data are in dB unit, i.e. they are given as $20\log_{10}|E|$.

3 Results and analysis

First, let us discuss our spectra presented as a function of the temperature difference $\Delta T = T_M - T_W$, under the condition of a fixed sum $(T_M + T_W)/2$ (Fig. 2). Without any interaction between both crystals, one expects a crossing of the AFMR modes in both crystals at $\Delta T = 0$. For example, such a crossing is observed in Fig. 2a at about 226 GHz, a frequency dictated by temperature $(T_M + T_W)/2 \approx 336$ K. We also observed two Fabry-Perot cavity modes at about 211 and 248 GHz. They are strongly interacting with AFMR in each of the crystals, forming polariton states that are visible as avoided crossings. Results presented in Fig. 2b were obtained for a distance d of 0.64 mm, chosen because a frequency of a cavity mode (227 GHz) is close to the frequency of the crossing of the AFMR. As discussed below using simulations, the data in Fig. 5b correspond to strong coherent coupling of the AFMR modes in both crystals. The strength of this coupling is larger than the strengths of the coupling when only one of the crystals is resonant with a cavity mode (Fig. 2a). This indicates that the resonance in the two crystals are cooperatively coupled to a cavity mode. The right panel (Fig. 2c) shows data obtained for $d = 0.83$ mm, which again presents almost unperturbed crossing of the AFMR modes as expected because the cavity mode is not resonant with the

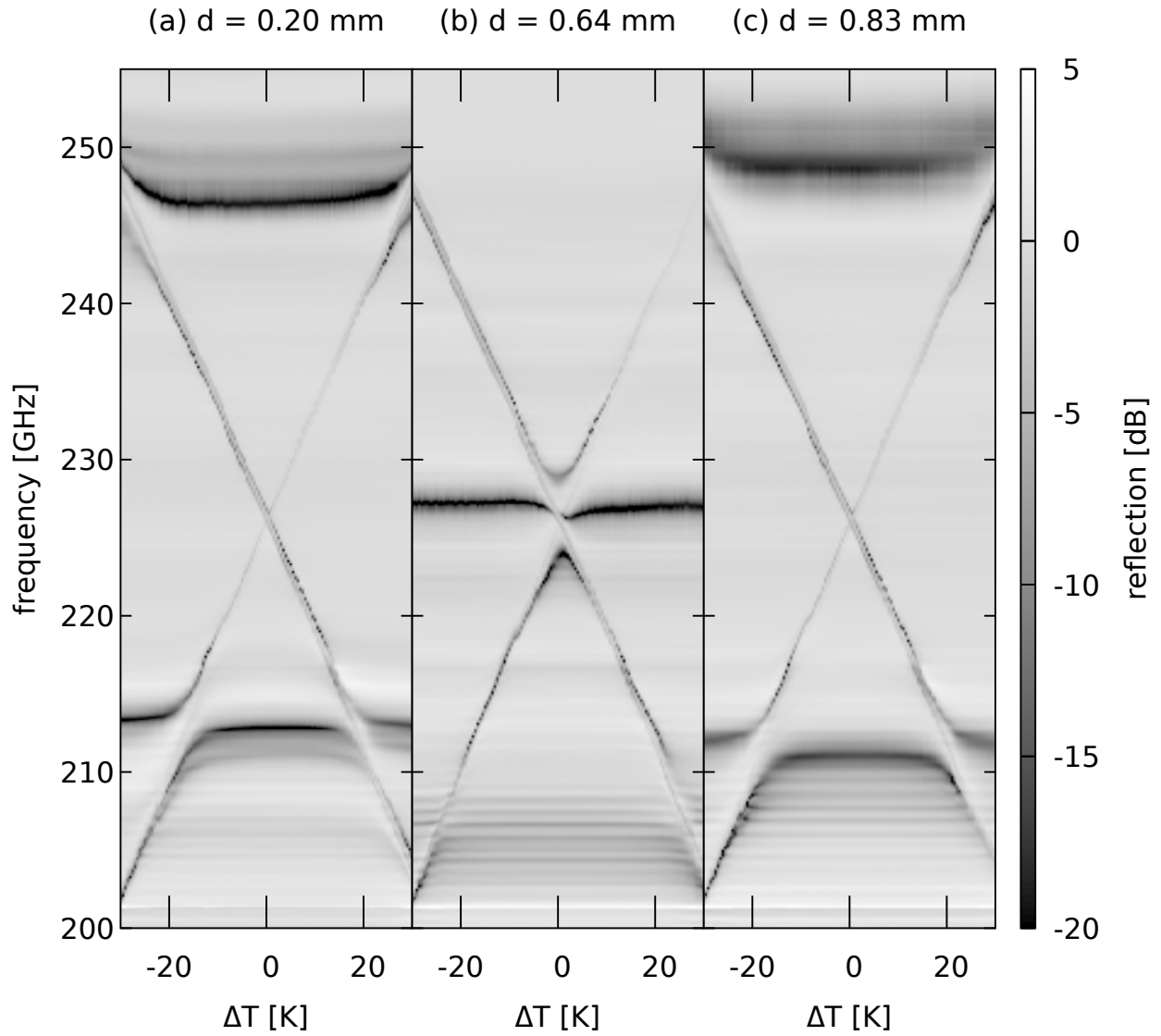


Figure 2: Normalized reflection magnitude at three different lengths of a gap d between the crystals obtained for $(T_M + T_W)/2 = 336$ K that results in the crossing point at $f \approx 227$ GHz.

AFMR frequency at the crossing. Thus, the coupling between the AFMR in both crystals depends on the distance between the crystals and the strength of this coupling has local maxima when the frequency of one of the cavity modes coincides with the crossing point.

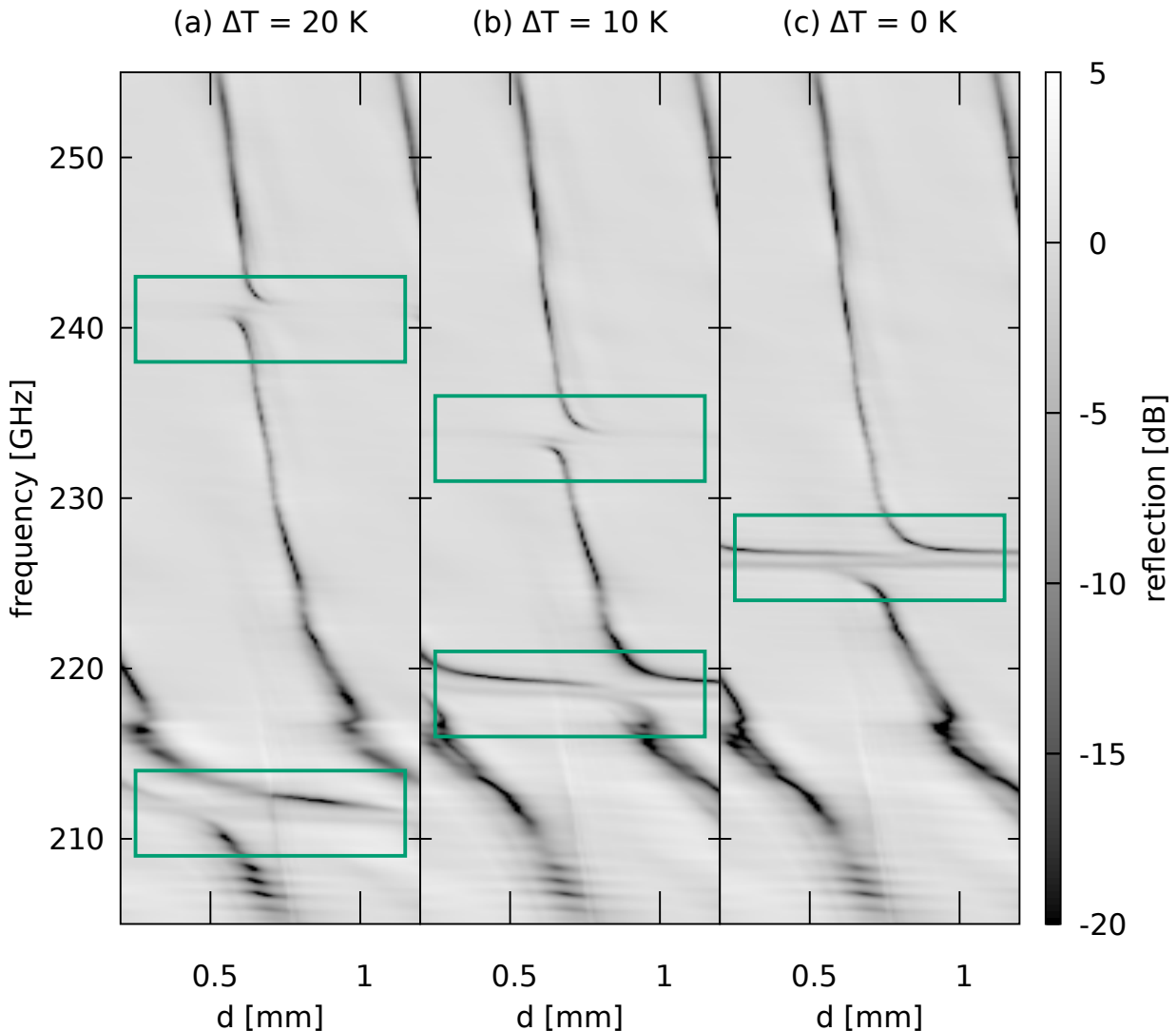


Figure 3: Normalized reflection magnitude at three temperature differences ΔT as a function of gap d between the crystals. Green rectangles mark strong couplings of AFMR with cavity modes. This result comes from the same data set as those in Fig. 2.,

Second, let us examine the data in Fig. 3 which present reflection as a function of air gap d for several set temperature differences. Note that the data shown in both Fig. 2 and 3 were extracted from one measurement run during which both ΔT and d were varied independently. With rising distance, one might expect a monotonic drop of cavity mode frequencies. In

Fig. 3, we can see instead formation of avoided crossing and gaps at the frequencies of AFMR in either one of the crystals (regions bordered with green rectangles). This result is a demonstration of the photonic character of the observed polariton modes, while the result as a function of temperature difference (Fig. 2) shows their magnonic character. In Fig. 3 we can see again that the splitting between the polariton modes is larger for $\Delta T = 0$ (Fig. 3c) than for couplings when only one of the crystals is on the resonance with the cavity mode (Fig. 3ab).

Let us now discuss our results in the context of three models: a model based on an input-output theory, a model using classical electrodynamics and a microscopic model.

3.1 Input-output theory

In the framework of the input-output theory,^{8,50,56} according to which a strongly coupled system is modelled as an RLC circuit with L containing a resonant term. As shown in Fig. 4b, we could account for the observed spectra (Fig. 4a) using:

$$S_{11} = 1 - a \left(i(f - f_c) - \frac{\kappa}{2} + \sum_{j=M}^W \frac{G_j^2}{i(f - f_j(T_j)) - \frac{w}{2}} \right)^{-1} \quad (1)$$

where, $a = -1.6$ GHz is a parameter describing the coupling of the cavity with the source and the detector, $f_c = 225.5$ GHz is the frequency of the cavity mode and $\kappa = 3.2$ GHz describes its width, $2G_W = 3.6$ GHz and $2G_M = 4.8$ GHz are, respectively, splittings between polariton branches for the AFMR in the crystals fixed on the waveguide and on the mirror, and $w = 0.7$ GHz describes AFMR width. Normalized coupling strengths are $\eta_W = 2G_W/f_c = 0.016$ and $\eta_M = 2G_M/f_c = 0.021$. We find that the observed coupling strength between AFMR modes in the two crystals at $\Delta T = 0$ is larger than coupling strengths with single crystals and that the magnon-magnon coupling $G_{mm} \approx \sqrt{G_W^2 + G_M^2} \approx 6$ GHz. This suggests that spins in both crystals are adding up to interact cooperatively with the cavity field.

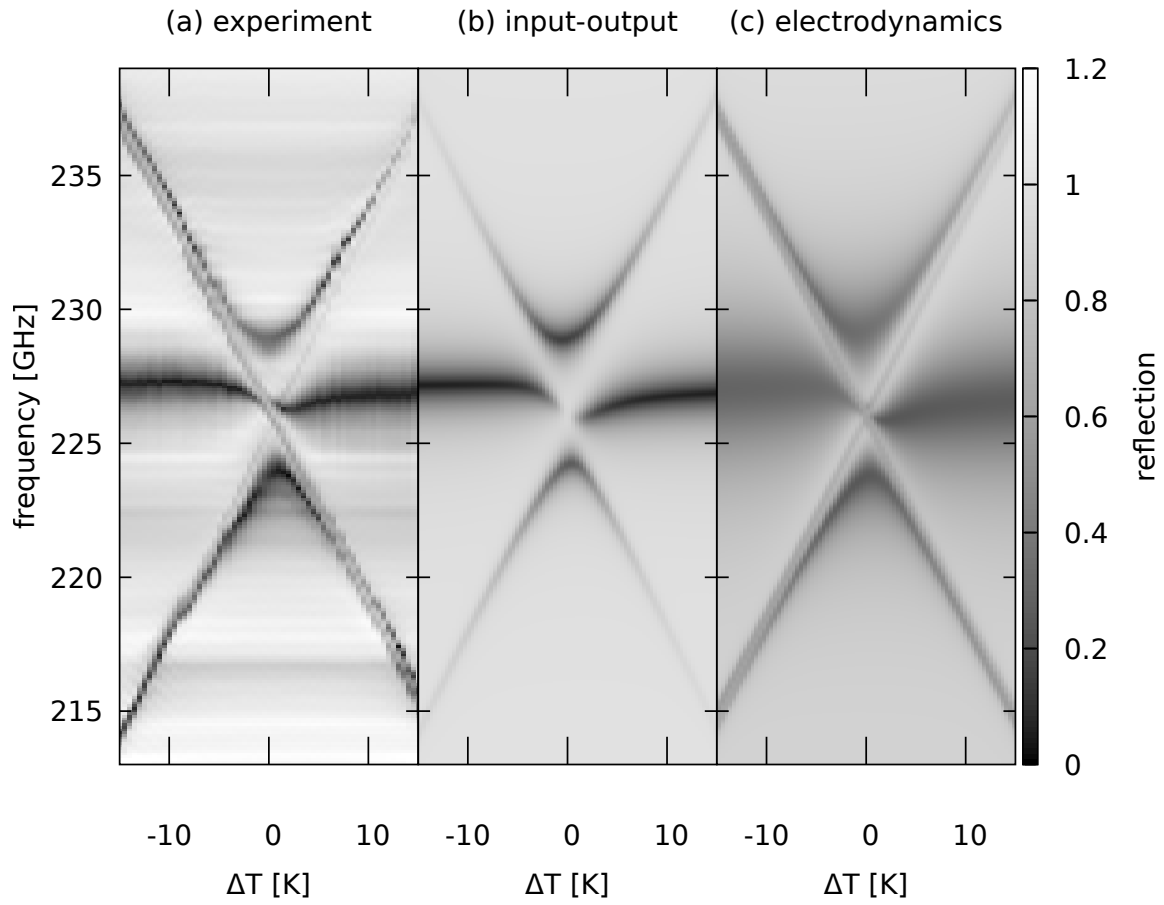


Figure 4: (a) Close-up of observed interaction region, (b) fit of an input-output model (Eq. 1) and (c) predicted reflection using the electrodynamic model.

3.2 Electrodynamics model

Classical electrodynamics allows analytical calculations of reflection from a system consisting of a series of parallel-plane slabs using characteristic matrix model for isotropic media.⁵⁷ Although hematite crystal is not isotropic, the off-diagonal terms in μ or ϵ are zero around the AFMR frequency.⁵⁸ Thus, for our calculations, we can assume an isotropic dielectric constant $\epsilon = 18.5$ for hematite ($\epsilon_{air} = 1$ for air). We take into account the antiferromagnetic resonance in the permeability, writing,

$$\mu = 1 + \frac{\Delta\mu f_r^2}{f_r^2 - f^2 - ifw}, \quad (2)$$

where f_r is its frequency, $w = 0.4$ GHz is its width and its strength $\Delta\mu = 0.9^{-3}$ as determined in our transmission results.³⁸ The strength of the resonance $\Delta\mu$ is responsible for the strength of the coupling of spin waves with electromagnetic waves. In the electrodynamics model, we neglect reflection from the metal mirror, since our calculations show that strong coupling originate from the constructive interference in the crystals themselves. For details please refer to the supplemental material.

The predicted reflection spectra are shown in Fig. 4c for gap $d = 700$ μm and crystals thicknesses of $h_M = 390$ μm and $h_W = 500$ μm . The electrodynamics model systematically predicts larger line widths of cavity modes than those observed in the experiment (Fig. 4a). This could be explained as an effect of elements of the experimental setup that cannot be taken into account by our one-dimensional model or the mirror that we neglect. In comparison with the model based on the input-output theory, the benefit of using the electrodynamics model is that it naturally takes into account the presence of other cavity modes and can account for absorption by the matter modes. Thus, in the electrodynamics model, we can account for the observed narrow lines in the middle of the interaction region that do not undergo avoided crossing.

3.3 Microscopic model

In order to analyze our data in terms of the quantum mechanism of light-matter coupling,¹⁰ we estimate the strength of the magnon-photon coupling with

$$G_j = \frac{g_s \mu_B}{2h} \sqrt{\frac{\mu_0 h V_s}{2 V_c} \rho f_c}, \quad (3)$$

where, $g_s = 2$, $\rho = 5\rho_{Fe}$ is the density of spins in hematite, where $\rho_{Fe} = 3.987 \times 10^{28} \text{ m}^{-3}$ is the density of iron atoms⁵⁹ and the factor 5 is the magnetic moment of Fe^{3+} ions.⁶⁰ The factor V_s/V_c describes the ratio of the j -th crystal volume to the volume of the entire cavity, which in the case of this experiment is of the order of $h_j/(h_1 + h_2 + d) < 0.5$. The expected splittings calculated this way ($2G_j$) are about an order of magnitude larger than the observed splittings (6 GHz). This discrepancy could be understood with Eq. 3 as being caused by only a small number of antiferromagnetic magnons interacting with THz photons. Classically, this can be understood as a small spatial overlap of a cavity mode magnetic field with the antiferromagnetic spin wave mode. In our case, determining this overlap is beyond the microscopic model.

In Fig. 5(a-d), we show results obtained over a large distance d with a step equal to an integer number of half a wavelength of the crossing frequency, which was set to about 244.5 GHz for this experiment. We observed that the coupling drops with increasing gap (Fig. 5(a-d)) and at above about $d \approx 10$ mm it is difficult to recognize the splitting between the three modes (Fig. 5(d)). We used the electrodynamics model (Fig. 5(e-h)) to explain the observed decrease in the splitting with increasing gap (Fig. 5(i)). This model also predicts that the quality factor of the cavity mode increases with increasing gap. Figure 5(i) shows the splitting between the low and high modes as a function of gap distance d . Assuming that the coupling should be proportional to the square root of the mean density of oscillators in

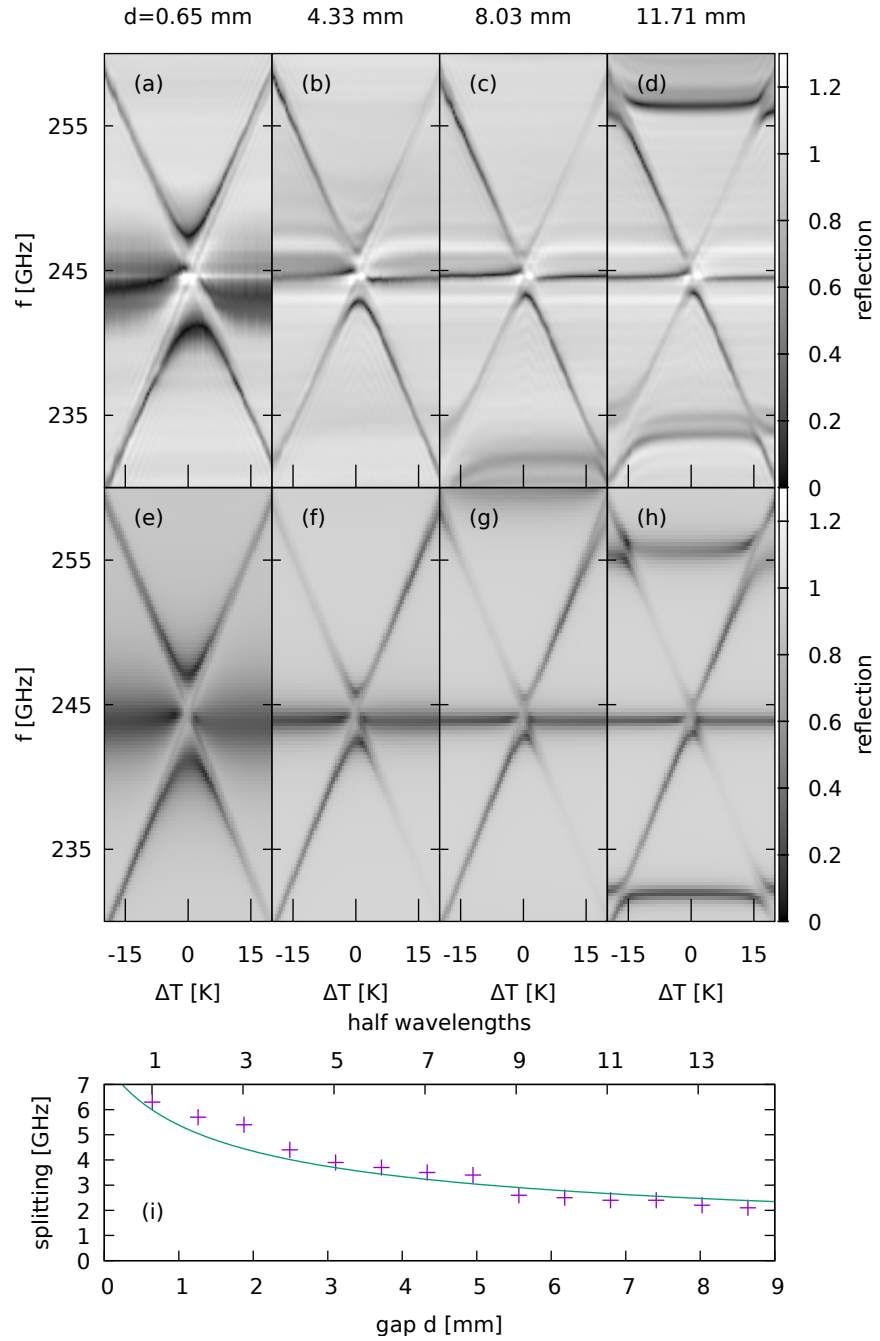


Figure 5: Top panels (a)-(d) show measured interactions at four selected distances between the crystals, which were equal to integer numbers of half wavelengths. The middle panels (e)-(h) show simulated reflection using the electrodynamic model. The bottom panel (i) shows splitting between the upper and lower magnon-polariton modes as a function of gap d between the crystals; the solid green line is a fit using Eq. 4.

the cavity, we could account for the data using,

$$G_{mm}(d) = G_{mm}^{(d=0)} \sqrt{\frac{d_0}{d_0 + d}}, \quad (4)$$

which yielded $d_0 = 0.9 \pm 0.2$ mm and $G_{mm}(d = 0) = (7.9 \pm 0.6)$ GHz. The fit value d_0 coincides with the sum of the actual crystal thicknesses $h_M + h_W = 0.89$ mm. This proves the general rule of proportionality of the coupling strength to the square root of the mean density of oscillators in the entire cavity.

4 Summary

We presented systematic experimental and theoretical studies of interaction of two magnetic polariton systems as a function of temperature and distance. Cooperative interaction of the magnetic polariton modes in the space-separated hematite (α -Fe₂O₃) crystals mediated by cavity mode was demonstrated and the characteristic interaction length was determined to be about ten times the sum of their thicknesses. The experiments were performed above room temperature and distances were in the mm range, i.e. quite a convenient range. This work shows that cavity-mediated coupling enables controlling antiferromagnetic polaritons by modulating a resonator surroundings, and allows construction of hybrid THz resonators that would share properties of their components.

Acknowledgement

Support by the Sino-Swiss Science and Technology Cooperation (SSSTC) grant no. EG-CN_02_032019 is gratefully acknowledged. The VNA and frequency extenders were funded by EPFL and the SNF R'Equip under Grant No. 206021_144983. Partial funding from the European Union's Horizon 2020 research and innovation programme under the Marie Skłodowska-Curie grant agreement No. 847639 and from the Ministry of Education and

Science of Poland is acknowledged. This work was also partially supported by the “International Research Agendas” program of the Foundation for Polish Science, co-financed by the European Union under the European Regional Development Fund (No. MAB/2018/9).

References

- (1) Törmä, P.; Barnes, W. L. Strong coupling between surface plasmon polaritons and emitters: a review. *Reports on Progress in Physics* **2014**, *78*, 013901.
- (2) Raizen, M. G.; Thompson, R. J.; Brecha, R. J.; Kimble, H. J.; Carmichael, H. J. Normal-mode splitting and linewidth averaging for two-state atoms in an optical cavity. *Phys. Rev. Lett.* **1989**, *63*, 240–243.
- (3) Khitrova, G.; Gibbs, H. M.; Kira, M.; Koch, S. W.; Scherer, A. Vacuum Rabi splitting in semiconductors. *Nature Physics* **2006**, *2*, 81–90.
- (4) Colombe, Y.; Steinmetz, T.; Dubois, G.; Linke, F.; Hunger, D.; Reichel, J. Strong atom–field coupling for Bose–Einstein condensates in an optical cavity on a chip. *Nature* **2007**, *450*, 272–276.
- (5) Basov, D. N.; Fogler, M. M.; de Abajo, F. J. G. Polaritons in van der Waals materials. *Science* **2016**, *354*, aag1992.
- (6) Bayer, A.; Pozimski, M.; Schambeck, S.; Schuh, D.; Huber, R.; Bougeard, D.; Lange, C. Terahertz Light–Matter Interaction beyond Unity Coupling Strength. *Nano Letters* **2017**, *17*, 6340–6344.
- (7) Roberts, R. W.; Auld, B. A.; Schell, R. R. Magnetodynamic Mode Ferrite Amplifier. *Journal of Applied Physics* **1962**, *33*, 1267–1268.
- (8) Schuster, D. I.; Sears, A. P.; Ginossar, E.; DiCarlo, L.; Frunzio, L.; Morton, J. J. L.; Wu, H.; Briggs, G. A. D.; Buckley, B. B.; Awschalom, D. D.; Schoelkopf, R. J. High-

- Cooperativity Coupling of Electron-Spin Ensembles to Superconducting Cavities. *Phys. Rev. Lett.* **2010**, *105*, 140501.
- (9) Abe, E.; Wu, H.; Ardavan, A.; Morton, J. J. L. Electron spin ensemble strongly coupled to a three-dimensional microwave cavity. *Applied Physics Letters* **2011**, *98*, 251108.
- (10) Huebl, H.; Zollitsch, C. W.; Lotze, J.; Hocke, F.; Greifenstein, M.; Marx, A.; Gross, R.; Goennenwein, S. T. B. High Cooperativity in Coupled Microwave Resonator Ferrimagnetic Insulator Hybrids. *Phys. Rev. Lett.* **2013**, *111*, 127003.
- (11) Zhang, X.; Zou, C.-L.; Jiang, L.; Tang, H. X. Strongly Coupled Magnons and Cavity Microwave Photons. *Phys. Rev. Lett.* **2014**, *113*, 156401.
- (12) Tabuchi, Y.; Ishino, S.; Ishikawa, T.; Yamazaki, R.; Usami, K.; Nakamura, Y. Hybridizing Ferromagnetic Magnons and Microwave Photons in the Quantum Limit. *Phys. Rev. Lett.* **2014**, *113*, 083603.
- (13) Tabuchi, Y.; Ishino, S.; Noguchi, A.; Ishikawa, T.; Yamazaki, R.; Usami, K.; Nakamura, Y. Coherent coupling between a ferromagnetic magnon and a superconducting qubit. *Science* **2015**, *349*, 405–408.
- (14) Zhang, X.; Zou, C.-L.; Zhu, N.; Marquardt, F.; Jiang, L.; Tang, H. X. Magnon dark modes and gradient memory. *Nature Communications* **2015**, *6*, 8914.
- (15) Zhang, X.; Zhu, N.; Zou, C.-L.; Tang, H. X. Optomagnonic Whispering Gallery Microresonators. *Phys. Rev. Lett.* **2016**, *117*, 123605.
- (16) Li, Y. et al. Strong Coupling between Magnons and Microwave Photons in On-Chip Ferromagnet-Superconductor Thin-Film Devices. *Phys. Rev. Lett.* **2019**, *123*, 107701.
- (17) Potts, C. A.; Davis, J. P. Strong magnon–photon coupling within a tunable cryogenic microwave cavity. *Applied Physics Letters* **2020**, *116*, 263503.

- (18) Lachance-Quirion, D.; Wolski, S. P.; Tabuchi, Y.; Kono, S.; Usami, K.; Nakamura, Y. Entanglement-based single-shot detection of a single magnon with a superconducting qubit. *Science* **2020**, *367*, 425–428.
- (19) Li, Y.; Zhang, W.; Tyberkevych, V.; Kwok, W.-K.; Hoffmann, A.; Novosad, V. Hybrid magnonics: Physics, circuits, and applications for coherent information processing. *Journal of Applied Physics* **2020**, *128*, 130902.
- (20) Bhoi, B.; Jang, S.-H.; Kim, B.; Kim, S.-K. Broadband photon–magnon coupling using arrays of photon resonators. *Journal of Applied Physics* **2021**, *129*, 083904.
- (21) Kasprzak, J.; Richard, M.; Kundermann, S.; Baas, A.; Jeambrun, P.; Keeling, J. M. J.; Marchetti, F. M.; Szymańska, M. H.; André, R.; Staehli, J. L.; Savona, V.; Littlewood, P. B.; Deveaud, B.; Dang, L. S. Bose–Einstein condensation of exciton polaritons. *Nature* **2006**, *443*, 409–414.
- (22) Awschalom, D. D.; Flatté, M. E. Challenges for semiconductor spintronics. *Nature Physics* **2007**, *3*, 153–159.
- (23) Dovzhenko, D. S.; Ryabchuk, S. V.; Rakovich, Y. P.; Nabiev, I. R. Light–matter interaction in the strong coupling regime: configurations, conditions, and applications. *Nanoscale* **2018**, *10*, 3589–3605.
- (24) Kockum, A. F.; Miranowicz, A.; De Liberato, S.; Savasta, S.; Nori, F. Ultrastrong coupling between light and matter. *Nature Reviews Physics* **2019**, *1*, 19–40.
- (25) Roux, K.; Konishi, H.; Helson, V.; Brantut, J.-P. Strongly correlated Fermions strongly coupled to light. *Nature Communications* **2020**, *11*, 2974.
- (26) Yuan, H.; Cao, Y.; Kamra, A.; Duine, R. A.; Yan, P. Quantum magnonics: When magnon spintronics meets quantum information science. *Physics Reports* **2022**, *965*,

- 1–74, Quantum magnonics: When magnon spintronics meets quantum information science.
- (27) Spethmann, N.; Kohler, J.; Schreppler, S.; Buchmann, L.; Stamper-Kurn, D. M. Cavity-mediated coupling of mechanical oscillators limited by quantum back-action. *Nature Physics* **2016**, *12*, 27–31.
- (28) Xu, P.-C.; Rao, J. W.; Gui, Y. S.; Jin, X.; Hu, C.-M. Cavity-mediated dissipative coupling of distant magnetic moments: Theory and experiment. *Phys. Rev. B* **2019**, *100*, 094415.
- (29) Li, Y.; Yefremenko, V. G.; Lisovenko, M.; Trevillian, C.; Polakovic, T.; Cecil, T. W.; Barry, P. S.; Pearson, J.; Divan, R.; Tyberkevych, V.; Chang, C. L.; Welp, U.; Kwok, W.-K.; Novosad, V. Coherent Coupling of Two Remote Magnonic Resonators Mediated by Superconducting Circuits. *Phys. Rev. Lett.* **2022**, *128*, 047701.
- (30) Wang, H.; He, W.; Yuan, R.; Wang, Y.; Wang, J.; Zhang, Y.; Medlej, I.; Chen, J.; Yu, G.; Han, X.; Ansermet, J.-P.; Yu, H. Hybridized propagating spin waves in a CoFeB/IrMn bilayer. *Phys. Rev. B* **2022**, *106*, 064410.
- (31) Harvey-Collard, P.; Dijkema, J.; Zheng, G.; Sammak, A.; Scappucci, G.; Vander-sypen, L. M. K. Coherent Spin-Spin Coupling Mediated by Virtual Microwave Photons. *Phys. Rev. X* **2022**, *12*, 021026.
- (32) Nair, J. M. P.; Mukhopadhyay, D.; Agarwal, G. S. Cavity-mediated level attraction and repulsion between magnons. *Phys. Rev. B* **2022**, *105*, 214418.
- (33) Yang, Z.-B.; Liu, H.-Y.; Yang, R.-C. Asymmetric quantum synchronization generation in antiferromagnet-cavity systems. *The European Physical Journal Plus* **2022**, *137*, 878.
- (34) Liensberger, L.; Kamra, A.; Maier-Flaig, H.; Geprägs, S.; Erb, A.; Goennenwein, S. T. B.; Gross, R.; Belzig, W.; Huebl, H.; Weiler, M. Exchange-Enhanced Ultrastrong

- Magnon-Magnon Coupling in a Compensated Ferrimagnet. *Phys. Rev. Lett.* **2019**, *123*, 117204.
- (35) Lebrun, R.; Ross, A.; Gomonay, O.; Baltz, V.; Ebels, U.; Barra, A.-L.; Qaiumzadeh, A.; Brataas, A.; Sinova, J.; Kläui, M. Long-distance spin-transport across the Morin phase transition up to room temperature in ultra-low damping single crystals of the antiferromagnet α -Fe₂O₃. *Nature Communications* **2020**, *11*, 6332.
- (36) Fischer, J.; Althammer, M.; Vlietstra, N.; Huebl, H.; Goennenwein, S. T.; Gross, R.; Geprägs, S.; Opel, M. Large Spin Hall Magnetoresistance in Antiferromagnetic α -Fe₂O₃/Pt Heterostructures. *Phys. Rev. Applied* **2020**, *13*, 014019.
- (37) Wang, H.; Xiao, Y.; Guo, M.; Lee-Wong, E.; Yan, G. Q.; Cheng, R.; Du, C. R. Spin Pumping of an Easy-Plane Antiferromagnet Enhanced by Dzyaloshinskii–Moriya Interaction. *Phys. Rev. Lett.* **2021**, *127*, 117202.
- (38) Białek, M.; Zhang, J.; Yu, H.; Ansermet, J.-P. Antiferromagnetic resonance in α -Fe₂O₃ up to its Néel temperature. *Applied Physics Letters* **2022**, *121*, 032401.
- (39) Jungwirth, T.; Sinova, J.; Manchon, A.; Marti, X.; Wunderlich, J.; Felser, C. The multiple directions of antiferromagnetic spintronics. *Nature Physics* **2018**, *14*, 200–203.
- (40) Hoffmann, A.; Bader, S. D. Opportunities at the Frontiers of Spintronics. *Phys. Rev. Applied* **2015**, *4*, 047001.
- (41) Li, J.; Wilson, C. B.; Cheng, R.; Lohmann, M.; Kavand, M.; Yuan, W.; Aldosary, M.; Agladze, N.; Wei, P.; Sherwin, M. S.; Shi, J. Spin current from sub-terahertz-generated antiferromagnetic magnons. *Nature* **2020**, *578*, 70–74.
- (42) Li, J.; Simensen, H. T.; Reitz, D.; Sun, Q.; Yuan, W.; Li, C.; Tserkovnyak, Y.; Brataas, A.; Shi, J. Observation of Magnon Polarons in a Uniaxial Antiferromagnetic Insulator. *Phys. Rev. Lett.* **2020**, *125*, 217201.

- (43) Reitz, D.; Li, J.; Yuan, W.; Shi, J.; Tserkovnyak, Y. Spin Seebeck effect near the antiferromagnetic spin-flop transition. *Phys. Rev. B* **2020**, *102*, 020408.
- (44) Ghosh, A.; Palit, M.; Maity, S.; Dwij, V.; Rana, S.; Datta, S. Spin-phonon coupling and magnon scattering in few-layer antiferromagnetic FePS₃. *Phys. Rev. B* **2021**, *103*, 064431.
- (45) Everts, J. R.; King, G. G. G.; Lambert, N. J.; Kocsis, S.; Rogge, S.; Longdell, J. J. Ultrastrong coupling between a microwave resonator and antiferromagnetic resonances of rare-earth ion spins. *Phys. Rev. B* **2020**, *101*, 214414.
- (46) Grishunin, K.; Huisman, T.; Li, G. Q.; Mishina, E.; Rasing, T.; Kimel, A. V.; Zhang, K.; Jin, Z. M.; Cao, S. X.; Ren, W.; Ma, G. H.; Mikhaylovskiy, R. V. Terahertz Magnon-Polaritons in TmFeO₃. *ACS Photonics* **2018**, *5*, 1375–1380.
- (47) Shi, L. Y.; Wu, D.; Wang, Z. X.; Lin, T.; Hu, C. M.; Wang, N. L. Revealing ultrastrong magnon-photon coupling in a polar antiferromagnet Fe₂Mo₃O₈ by time domain terahertz spectroscopy. 2020.
- (48) Li, X.; Bamba, M.; Yuan, N.; Zhang, Q.; Zhao, Y.; Xiang, M.; Xu, K.; Jin, Z.; Ren, W.; Ma, G.; Cao, S.; Turchinovich, D.; Kono, J. Observation of Dicke cooperativity in magnetic interactions. *Science* **2018**, *361*, 794–797.
- (49) Sivaraajah, P.; Steinbacher, A.; Dastrup, B.; Lu, J.; Xiang, M.; Ren, W.; Kamba, S.; Cao, S.; Nelson, K. A. THz-frequency magnon-phonon-polaritons in the collective strong-coupling regime. *Journal of Applied Physics* **2019**, *125*, 213103.
- (50) Białek, M.; Zhang, J.; Yu, H.; Ansermet, J.-P. Strong Coupling of Antiferromagnetic Resonance with Subterahertz Cavity Fields. *Phys. Rev. Applied* **2021**, *15*, 044018.
- (51) Jarc, G.; Mathengattil, S. Y.; Giusti, F.; Barnaba, M.; Singh, A.; Montanaro, A.; Glerean, F.; Rigoni, E. M.; Zilio, S. D.; Winnerl, S.; Fausti, D. Tunable cryogenic tera-

- hertz cavity for strong light–matter coupling in complex materials. *Review of Scientific Instruments* **2022**, *93*, 033102.
- (52) Caspers, C.; Gandhi, V. P.; Magrez, A.; de Rijk, E.; Ansermet, J.-P. Sub-terahertz spectroscopy of magnetic resonance in BiFeO₃ using a vector network analyzer. *Applied Physics Letters* **2016**, *108*, 241109.
- (53) Białek, M.; Ito, T.; Rønnow, H.; Ansermet, J.-P. Terahertz-optical properties of a bismuth ferrite single crystal. *Phys. Rev. B* **2019**, *99*, 064429.
- (54) Białek, M.; Magrez, A.; Ansermet, J.-P. Spin-wave coupling to electromagnetic cavity fields in dysprosium ferrite. *Phys. Rev. B* **2020**, *101*, 024405.
- (55) Zhang, J.; Białek, M.; Magrez, A.; Yu, H.; Ansermet, J.-P. Antiferromagnetic resonance in TmFeO₃ at high temperatures. *Journal of Magnetism and Magnetic Materials* **2021**, *523*, 167562.
- (56) Harder, M.; Bai, L.-H.; Match, C.; Sirker, J.; Hu, C.-M. Study of the cavity-magnon-polariton transmission line shape. *Science China Physics, Mechanics & Astronomy* **2016**, *59*, 117511.
- (57) Born, M.; Wolf, E. In *Principles of Optics (Sixth Edition)*, sixth edition ed.; Born, M., Wolf, E., Eds.; Pergamon, 1980; pp 1 – 70.
- (58) Zavislyak, I.; Chumak, H. Tunable Reflective Structures Based on Weak Ferromagnetics and Their Application as Tunable Sub-Terahertz Resonators. *Radioelectronics and Communications Systems* **2019**, *63*, 377–390.
- (59) Pailhé, N.; Majimel, J.; Pechev, S.; Gravereau, P.; Gaudon, M.; Demourgues, A. Investigation of Nanocrystallized α -Fe₂O₃ Prepared by a Precipitation Process. *The Journal of Physical Chemistry C* **2008**, *112*, 19217–19223.

- (60) Shull, C. G.; Strauser, W. A.; Wollan, E. O. Neutron Diffraction by Paramagnetic and Antiferromagnetic Substances. *Phys. Rev.* **1951**, *83*, 333–345.